

Contents

| | | |
|----------|---|-----------|
| 1 | Introduction | 2 |
| 2 | Experimental Setup | 5 |
| 2.1 | Construction of the stable light path | 5 |
| 2.1.1 | CRL parameter determination | 5 |
| 2.1.2 | Reduce beam jitter | 7 |
| 2.2 | Construction of the combined system | 8 |
| 2.3 | Determination of spot parameters | 9 |
| 2.4 | Collection of micro-focus X-ray scattering data | 10 |
| 3 | Application | 11 |
| 3.1 | Microstructure of ringed spherulites | 11 |
| 3.2 | The skin and core structure of the fiber | 13 |
| 4 | Conclusion | 14 |

1

Abstract

2 SAXS technology is commonly used in the characterization of the microstructure of polymer materials. However,
3 the current common SAXS line station is limited by the size of the incident light spot, and its resolution cannot accurately
4 characterize the microstructure in the polymer system. At the same time, the general SAXS line station is not equipped
5 with an optical microscopy system, which cannot accurately correspond to the detection result with the actual structure.
6 The above problems restricts the research on polymer systems. To solve the above problems, it is necessary to obtain a
7 focused X-ray spot with a sufficiently small spatial resolution and to be able to determine the detection site in real-time
8 on the optical microscopy system. Compound refractive lenses are often used for synchrotron X-ray micro-focusing.
9 Polarized light microscopes are often used to observe the morphology of crystalline polymers. Based on this idea, an
10 optical system consisting of a compound refractive lens and a polarizing microscope is built-in this article. It is deployed
11 in the light path of the synchrotron radiation small-angle scattering line station, and through a series of adjustments. The

12 micro-focusing SAXS and the polarization microscopy system are combined. The feasibility of the whole system was
13 verified through the characterization experiment of the ringed-spherulite microdomain structure and the fiber sheath-core
14 structure. It provides a new characterization platform for the Shanghai Optical Small-Angle Scattering Line Station, and
15 a different combination structure characterization method for internal and external teams conducting polymer crystal
16 structure research.

17 **1 Introduction**

18 Macromolecules are characterized by their long-chain structure, including molecular chain unit and conformation on
19 the angstrom scale, lamella on the nanometer scale, and spherulites on the micron scale. Nowadays, synchrotron ra-
20 diation small-angle X-ray scattering (SAXS) and wide-angle X-ray diffraction (WAXD), as a non-destructive, highly
21 statistically averaged structure analysis method, have been extensively utilized in the crystalline polymer research area.
22 For instance, information on grains in the crystalline polymer, micro-domains in blended polymers and the shape, size,
23 and distribution of cavities and cracks can be obtained by Guinier scattering. Information on orientation, thickness, and
24 the crystalline fraction of the crystalline layer, and the thickness of the amorphous layer can be obtained by long-period
25 measurement.

26 The research of microstructure of polymer is fundamental to direct industrial applications of them. To further study
27 the internal structure of polymers, two test conditions are essential. Firstly, considering the size of a specific structural
28 unit, the size of the X-ray spot can not be too large. For instance, in spherulites research, an X-ray spot with a size
29 of $5\mu\text{m} \times 5\mu\text{m}$ is required. A small spot provides sufficient spatial resolution when the structure of macromolecules is
30 characterized by the SAXS method. Secondly, to match the characterization result with the real structure, it is a critical
31 measure to confirm the real-time exact position of the X-ray incident beam on polymer crystal.

32 As described, the X-ray spot needs to be focused and located.

33 To improve the spatial resolution of the synchrotron radiation experiment, nearly all the world's advanced syn-
34 chrotron radiation facilities focus the X-ray spot in the micron or even sub-micron level. Representative beamline
35 stations include PETRA III P03, SSRF BL15U1[1]. However, limited by the distance between the sample and the
36 detector, SAXS experiments can not be implemented on these stations. Consequently, it is necessary to build an inde-

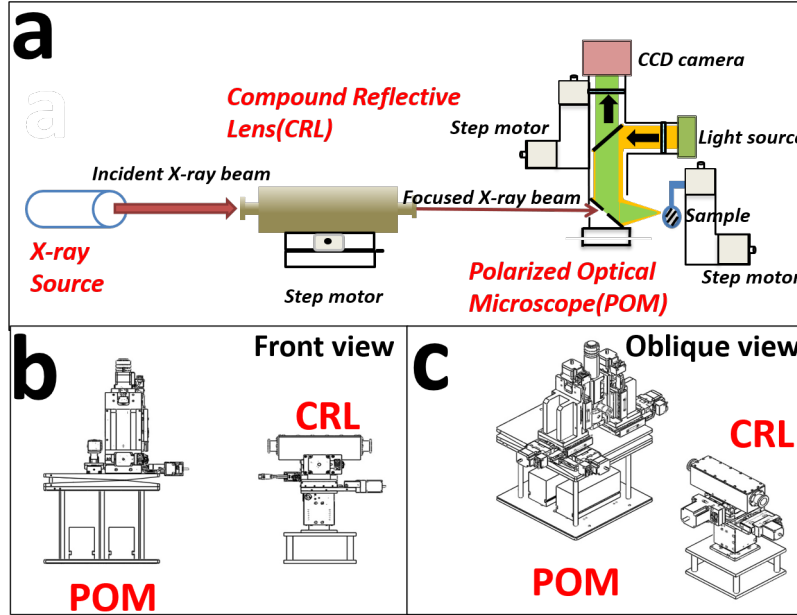


Fig. 1. Whole system.

37 pendent optical system with the functions of X-ray micro-focusing and precise spot positioning on the existing SAXS
38 beamline.

39 The main component used for X-ray beam focusing includes a Kirkpatrick-Baez mirror[2], Fresnel zone plates,
40 Capillary optical lens[3], and Compound refractive lenses[4, 5]. In the synchrotron radiation area, Kirkpatrick-Baez
41 mirror(K-B mirror) and Compound refractive lenses(CRL) are more widely used. In practice, advantages of K-B mirror
42 are aberration-free imaging on both horizontal and vertical planes, no dispersion, high energy, high reflectivity and low
43 flux losses. However, there are some non-negligible disadvantages. Micro-beam focusing by K-B mirror needs to be
44 achieved by adjusting the interval mirrors and multi-axis spatial attitude, including the angle of incident X-ray on the
45 mirrors, the vertical angle of the two mirrors, spatial parallelism of two vertical cylinders. The deployment of the K-B
46 mirror changes the original optical path. Thus, the K-B mirror, as an off-axis device, increases the complexity of the
47 installation of all the experimental equipment. This is unfavorable for the entire micro-focusing experiment process.

48 Compound refractive lenses(CRL) are comprised of a series of single lenses arranged in a linear array to achieve
49 X-ray focusing in the energy range of 5-40 keV. As shown in Fig. 2, the most widely used CRL is parabolic type. The

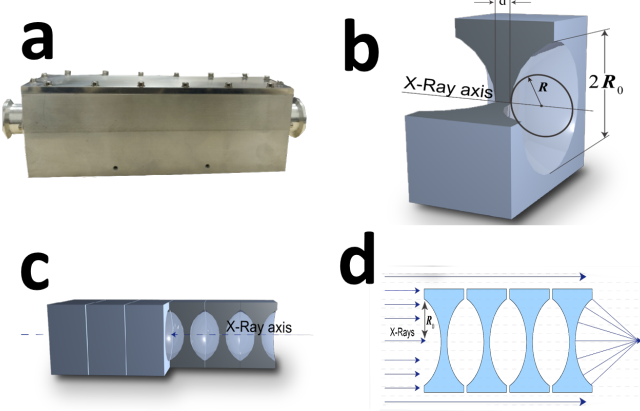


Fig. 2. Structure of Compound reflective lenses

50 parabolic CRL has a parabolic surface that rotates around the axis of symmetry to form a parabola. It can focus X-rays
 51 in two dimensions without causing aberrations in theory. Compared to the K-B mirror, CRL does not alter the original
 52 optical path propagation direction. CRL has excellent high-temperature stability, simple and compact structure and low
 53 requirements for lens surface roughness. Moreover, CRL is not difficult to adjust and relatively insensitive to vibration.
 54 The most obvious disadvantage of CRL is its low transmission efficiency. Owing to the small aperture of the diaphragm
 55 and the high absorbed rate of X-ray for CRL, the intensity of focused light will drop by one to two orders of magnitude
 56 than original light. Despite this, the luminous flux can be maintained at $10^{10} \sim 10^{11}$ phs/s after CRL micro-focusing.
 57 It can be proved in [subsubsection 2.1.1](#). This flux is enough for the structure research of crystalline polymers.

58 Polarized optical microscopy(POM) is commonly used in polymer crystal morphology research. POM is a simple
 59 method to distinguish the change of growth direction of crystals in the film plane and to check whether there exists
 60 twisting of crystals[6]. [Fig. 3](#) is a schematic diagram of the disassembly of a POM. When the polarized light generated
 61 by the polarizer and the analyzer enters the anisotropic polymer crystal, birefringence occurs, and the crystal contrast is
 62 provided by the coherence of the polarized light. Different crystal forms of polymers, such as spherulites, string crystals,
 63 stretched chain crystals, transverse crystals, etc., all have anisotropic optical properties, so their crystal morphology, size,
 64 number, etc. can be observed clearly with a POM.

65 The application of POM on a SAXS beamline had been a largely underexplored domain. In this passage, a com-
 66 bined system of micro-focusing SAXS and POM is proposed. Parameters of the system are optimized after a series

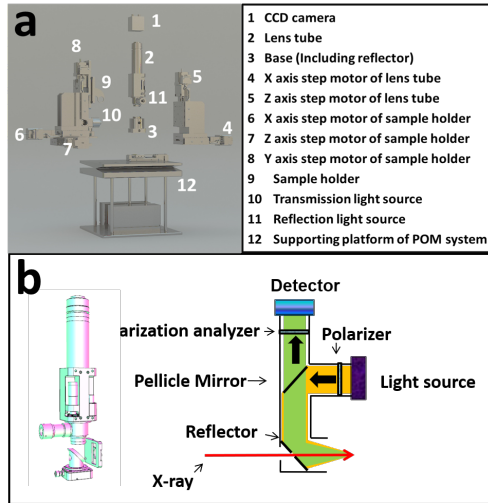


Fig. 3. POM overall disassembly and lens cone disassembly.

67 of calculations and experiments. The device is utilized to characterize the crystalline morphology and microstructure
68 of related polymers on a SAXS beamline. This study should make an important contribution to the field of polymer
69 morphological research.

70 **2 Experimental Setup**

71 **2.1 Construction of the stable light path**

72 **2.1.1 CRL parameter determination**

73 To obtain the designed X-ray microbeam, CRL's parameters are necessary to be determined first. The parameter mainly
74 includes material, geometric size, and the number of pieces. Commonly used CRL is aluminum and beryllium. Basing
75 on the theory of atomic physics, materials with low atomic numbers have less absorption of X-rays. In this system, a
76 beryllium CRL is chosen because the X-ray energy has to be preserved as much as possible.

77 There are three common single lenses. The main geometric parameters of them are listed in [Table 1](#). First, CRL
78 with a radius of $50 \mu\text{m}$ is selected to calculate the relevant parameters.

79 Transmittance refers to the ratio of the light intensity after passing through the lens and the light intensity without

Table 1. Parameters of several common single lens

| Radius $R/\mu\text{m}$ | Aperture $2R_0/\mu\text{m}$ | Area $\pi R_0^2/\text{mm}^{-2}$ |
|------------------------|-----------------------------|---------------------------------|
| 200 | 881 | 0.609 |
| 100 | 623 | 0.305 |
| 50 | 440 | 0.152 |

passing through the lens. It can be calculated by Eq. 1[7]:

$$T_p = \frac{\int_0^{2\pi} d\theta \int_0^{R_0} e^{-\mu ND(r)} r dr}{\int_0^{2\pi} d\theta \int_0^{R_0} r dr} = \frac{1 - e^{-a}}{a} e^{-\mu Nd} \quad (1)$$

In Eq. 1, $a = \mu NR_0^2/R$, R and R_o are given in Table 1, N is the number of lenses, d is the minimum thickness of a single mirror. For parabolic lenses, d can be calculated by Eq. 2:

$$D(r) = d + 2 \times \frac{r^2}{2R} \quad (2)$$

The maximum thickness $D(r)$ of the selected CRL is 2 mm. Substituting $D(r)$ and $r = R_0$ into the Eq. 2, d equals 1.032 mm.

Considering the actual situation of shed size and pipeline layout, the designed image distance is about 400 mm and so is the focal length. The focal length under the approximate condition of a thin lens can be calculated by Eq. 3 :

$$f = R/2N\delta \quad (3)$$

N is the number of lenses, δ is the real part of refractive index to 1 offset. δ can be calculated by Eq. 4 [8]:

$$\delta = \frac{2\pi\rho r_o}{k^2} \quad (4)$$

ρ is electron number density, r_o is the electronic classical radius and k is wave vector. For beryllium in 12KeV, δ is 2.36393×10^{-6} . When N is set to 30, the focal length is 352.5 mm. This value meets the requirements described above. Substituting $N = 30$ and $d = 1.032$ into the Eq. 1, T_p equals 0.327.

91 The flux of photons after passing through the lenses can be calculated by the following equation:

$$I = i \times T_p \times R \quad (5)$$

92 i is the flux of incident X-ray. In BL19U2, under a current intensity of 220 mA, $i = 2.5 \times 10^{12}$ photons/s, R is defined as
93 the photon acceptance rate and equals 0.0598 in BL19U2. Substituting these values into the [Eq. 5](#), I equals 4.89×10^{10}
94 photons/s. This value is enough to study the structure of crystalline polymers.

95 For a lens with a radius of 100 μm and 200 μm , after the same calculation, N is 60 and 120. Although a lens with a
96 larger radius of curvature can be used to obtain a slightly larger flux, the number of lenses required is greatly increased.
97 Comprehensive consideration, using 30 lenses with a radius of 50 μm is the best choice.

98 **2.1.2 Reduce beam jitter**

99 Due to the thermal load caused by the high-power beam to the monochromator crystal and the vibration of the monochro-
100 mator crystal caused by the liquid nitrogen cooling system of the monochromator, the current spot of the BL19U2 is
101 differed by about 10%, which will affect the strength stability of X-ray microbeam.

102 A processing software is compiled which integrates light intensity position data collection, data processing (cal-
103 culation of beam center), data smoothing and filtering, PID control algorithm and control interface. Advanced FPGA
104 technology is applicable to design and implement a fuzzy adaptive PID controller. Beam position which is collected by
105 the PID control loop in real-time is compared with the set value. Then the comparison error is sent to the PID controller
106 to calculate the control value through the PID control algorithm. Subsequently, the comparison error is input to the
107 actuator of the monochromator piezo to adjust the piezo angle of the second crystal in real-time. This operation realizes
108 the constant feedback system of the beam center position and the constant light intensity feedback system. Finally, it
109 is realized that the closed-loop control of the beam position and suppress low the beam drift of the frequency band to
110 realize the stabilization of the BL19U2. Thus, the impact of beam jitter on the intensity of the focused beam is lowered.

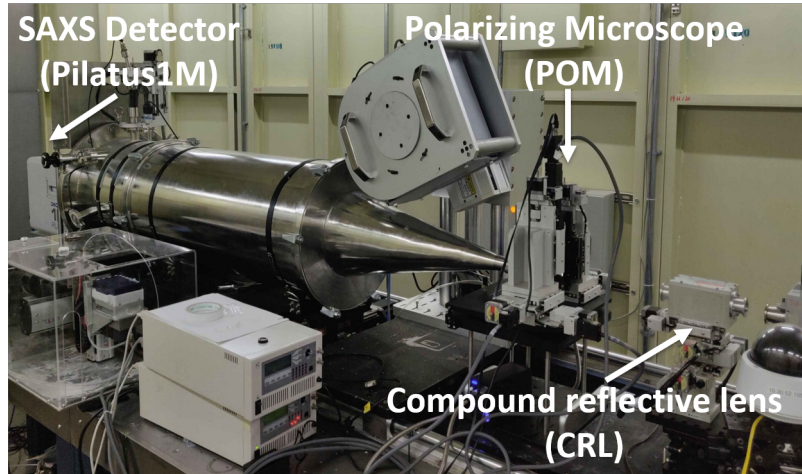


Fig. 4. Site map of the combined system.

2.2 Construction of the combined system

Fig. 1 is the schematic diagram of the structure of the synchrotron radiation X-ray micro-focusing polarized microscopy system. The combined system has one micro-focusing component and an in situ polarized light microscope system. After the incident X-ray is focused by the CRL, it will pass through the light hole on the lower side of the POM and the sample, then the scattered signal will be received by the detector. The on-site construction diagram of the system is shown in Fig. 4.

As shown in Fig. 1, the CRL is mounted on a motorized platform. The platform includes a three-dimensional translational electric platform (x , y , z three directions), one-dimensional swing stage (P angle), and one-dimensional rotating platform (R angle). The spatial posture of CRL can be adjusted in five dimensions.

The structure of the POM used in the system is shown in Fig. 3. As shown in Fig. 3b, the optical system of POM mainly consists of the following parts: a polarizer and analyzer that use ordinary white light sources to generate polarized light; a half mirror located in the middle of the lens barrel; A flat mirror located at the bottom of the lens barrel. The detector at the top is utilized to collect images. In this system, the detector selects a Charge-coupled device(CCD) camera.

As shown in Fig. 3a, the in situ POM system is also installed on a motorized support platform. A stepping motor (4~5) installed on the side of the lens body realizes the translational adjustment of the lens barrel in two dimensions.

127 Similarly, the stepping motor (6~8) on the side of the sample holder realizes its translational adjustment in three dimen-
128 sions. The supporting platform (12) can be further divided into three layers: the uppermost layer is a one-dimensional
129 swing stage and a rotating table, the middle layer is a two-dimensional (horizontal) translational electric platform, and
130 the lowest layer is a three-dimensional translational electric platform. Through the adjustment devices in all the above
131 dimensions, the five spatial dimensions of the entire optical system can be adjusted.

132 **2.3 Determination of spot parameters**

133 Once the combined system is installed in the beamline, the beam can be adjusted. The main purpose of beam adjustment
134 is threefold: first, to ensure the connectivity of the integrated optical path, to ensure that X-rays can pass through the
135 system correctly. A series of elements on the fixed light path of the beamline is used to adjust the primary light spot, and
136 then the light path is adjusted using the POM and CRL spatial dimensions. The current value of the ionization chamber
137 can determine whether there is sufficient X-ray flux to irradiate the sample. The second purpose is to verify whether
138 the CRL is accepted to focus the primary spot to sufficiently small spot size. Only when the size is basically in line
139 with the theoretical value to achieve a sufficiently small spatial resolution, can the microstructure of the research system
140 be characterized; the third is to adjust the position of the light spot to the center of the field of view while adjusting
141 the angle of the plane mirror to make the polarized light that reaches the sample after being reflected twice by the half
142 mirror and the plane mirror is focused on the X-ray at this point in the sample. The detection point of the sample is
143 placed in the center of the field of view, and the detection position will not shift even if the magnification of the polarizing
144 microscope is changed. To achieve the latter two purposes, we need to observe the spot in real-time under POM. For this
145 reason, we install a cesium iodide crystal on the sample stage. Cesium iodide crystal has the characteristic of emitting
146 fluorescence under X-rays, so it is also called scintillation crystal. In this system, the X-ray spot position is calibrated
147 by the fluorescence spectrum generated by cesium iodide under POM.

148 Step motors used in this system are all produced by Kohzu Corporation. Positioning accuracy can reach $1\mu\text{m}$,
149 which is enough for precise spatial position adjustment. Adjust the CRL posture so that the incident X-ray can pass
150 through the lenses correctly and be focused. Then adjust the y-direction motor of the POM sample stage, so that the
151 scintillation crystal is correctly focused and imaged in the field of view of the polarizing microscope. Finally, set the
152 x and z direction motors to move the center of the field of view to the fluorescent spot. In the PC imaging software, a

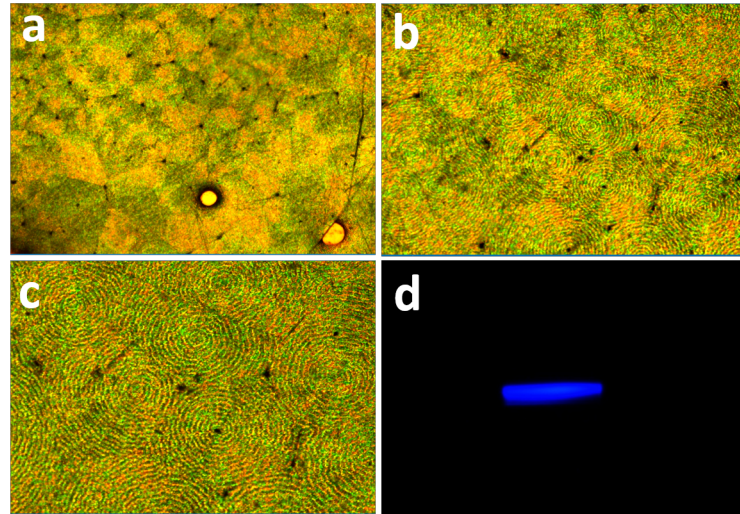


Fig. 5. Result of commissioning POM on site

153 cross ruler will be displayed to provide assistance in positioning.

154 The theoretical size of the focus spot is about $5\mu\text{m} \times 5\mu\text{m}$. In check to see whether the error between the actual size
 155 and the theoretical calculation is within the allowable range, two methods are used. As shown in Fig. 6a and Fig. 6b,
 156 the first is to visually observe through imaging software and use a ruler to make rough measurements. This method is
 157 fairly intuitive and fast, but the accuracy is insufficient. The second method is Gaussian fitting by using current data
 158 of the ionization chamber. Basing on related theories, the flux of X-rays determines the intensity of the current in the
 159 ionization chamber. FWHM of the $\frac{dI}{dx} \sim x$ curve(first derivative of the ionization chamber current to displacement)
 160 represents the spot size. Representative fitting results of this system are shown in Fig. 6c and Fig. 6d. The FWHM of
 161 the fitted peak is calculated to be $5.43\mu\text{m} \times 6.52\mu\text{m}$. This value achieves the expected effect.

162 **2.4 Collection of micro-focus X-ray scattering data**

163 After adjusting the size and position of the light spot, it can be utilized to characterize the micro-domain structure of
 164 related polymer crystals. First, determine the position that needs to be characterized under the POM, and then use the
 165 motor installed on the platform to remove the visible light source. The synchrotron X-rays pass through the CRL and
 166 focus to the required size, and then irradiate the sample through the light hole on the POM sample stage to collect the

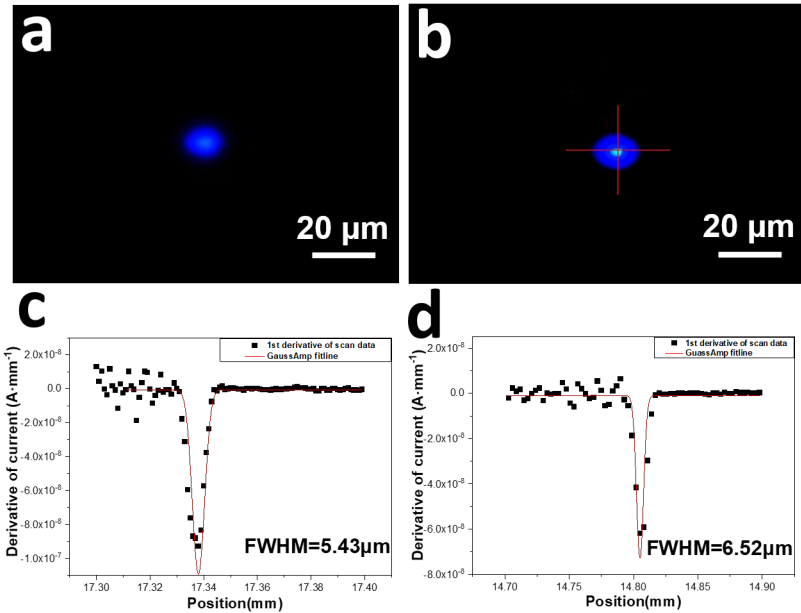


Fig. 6. Result of CRL micro-focus (facula and flux)

167 SAXS signal. At the SSRF-BL19U2 beamline, X-rays with an energy of 12keV are often utilized, and the distance be-
 168 tween the sample and the detector is 2700 mm. The scattering signal is collected by Pilatus1M detector (981×1043 pixel,
 169 with a pixel size of $172\mu\text{m} \times 172\mu\text{m}$).

170 **3 Application**

171 To verify the feasibility of the entire combined system, the spherulites with annulus and fibers with a sheath-core struc-
 172 ture are used as research examples. A micro-focused X-ray spot is used for micro-area resolution, and the scattering
 173 information of small structures that cannot be obtained by ordinary small-angle scattering experiments can be obtained.

174 **3.1 Microstructure of ringed spherulites**

175 Spherulites are the most common morphological structure of polymer materials, and they play a vital role in the physical,
 176 chemical, and mechanical properties of polymer materials. Its multi-level structure is complicated, and many basic
 177 scientific issues related to its structure have yet to be further explored. At present, in the study of the microstructure

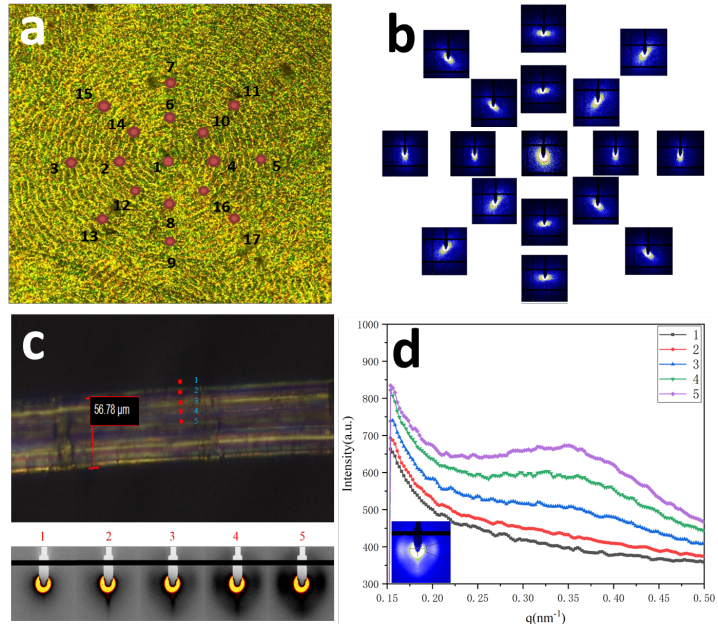


Fig. 7. The application sample of the system

of zonal spherulites, several scientific problems need to be explained urgently[9]. The first problem is the correlation between the growth axis of the polymer ring-belt spherulites and the torsion chirality of the lamellae. One theory is that the growth axis affects the chirality of the lamella torsion by changing the pressure distribution on the lamella plane. Micro-focus X-ray can be used to determine the growth axis of each region and the tilt torsion behavior of the mapping crystal plane along the growth axis, revealing the correlation between the crystal growth axis and the lamella torsion chirality. It can provide a scientific basis for clarifying the transfer behavior of chirality between the multi-level structure of polymer spherulites. The second problem is the cross nucleation of polymer spherulites during crystallization. Through micro-focus X-ray, the crystalline transformation information at the front of spherulite growth is monitored in situ, including crystal plane, orientation, whether there is a transition (gradient) zone to reveal the cross nucleation mechanism in polymer crystals, and clarify multiple crystal types the correlation and the similarities and differences between polymer cross nucleation and traditional cross nucleation of the small molecule.

Ringed-spherulites were chosen to verify the usability of the micro-focusing polarizing microscope system. Micro beam X-ray scans were especially informative. As shown in Fig. 7a, the initial growth site (1) of the ringed-spherulites was first calibrated, and the micro-focus SAXS characterization was performed on this point. Subsequently, 8 sites were

192 uniformly selected and characterized on a certain circumference of the ring-belt spherulites. To eliminate contingency,
 193 a total of 16 sites (2-17) in two different circles were selected, and SAXS characterization was also performed. The
 194 two-dimensional image of the SAXS result is shown in Fig. 7b, and it can be seen from Fig. 7b that the distribution of
 195 the scattering intensity at different sites is different. The scattering intensity at the center of the spherulites is equal in
 196 all directions. However, in all directions around the ringed-spherulites, there is a certain orientation, which also reflects
 197 the periodic changes in the arrangement of the lamellae on the ringed-spherulites.

198 The Herman factor of each characterized spot can be calculated as follows:

$$f_{or} = \frac{\int_0^{\frac{\pi}{2}} I(3\cos^2 \varphi - 1) \sin \varphi d\varphi}{2 \int_0^{\frac{\pi}{2}} I \sin \varphi d\varphi}. \quad (6)$$

199 Through the precise characterization of the ringed-spherulites by micro-focused X-rays, experimental results with certain
 200 differences have been obtained. The above examples can support the usability of the system.

201 3.2 The skin and core structure of the fiber

202 For fiber materials, the skin layer and the core layer of the fiber will have certain structural differences due to the
 203 temperature and shear flow field factors in the preparation process. Some fibers have small diameters, and conventional
 204 SAXS methods cannot accurately characterize the structure of the skin or core layer. The interval of taking points is
 205 about $5\mu\text{m}$. Micro-focused X-rays can accurately distinguish the skin layer from the core layer and even the transition
 206 layer, and use the scattering data to study the organizational differences.

207 As shown in Fig. 7c, the micro-beam X-rays irradiate the detection points of the skin and core of the fiber. The
 208 corresponding scattering data is shown in Fig. 7d. It can be seen from the $I(q)$ - q curve that there is also a significant
 209 difference in the peak scattering intensity of the skin layer and the core layer. In order to elucidate the difference of
 210 the skin layer and core layer of high density polythene(HDPE) fiber, one-dimensional scattering intensity distribution
 211 along the depth direction are characterized. (Fig.8). The average thickness of the crystalline lamellae and amorphous
 212 layer measured along the depth direction of fibers can be derived from the one-dimensional electron density correlation
 213 functions $K(z)$ as follows:

$$K(z) = \frac{\int_o^\infty I(q)q^2 \cos(qz) dq}{\int_o^\infty I(q)q^2 dq} \quad (7)$$

214 Simultaneously, the difference in image brightness caused by the structural differences of each part of the fiber can also
215 be observed under a POM.

216 In the two demonstrations of ringed spherulites and fibers with skin-core structure, through the micro-focusing
217 polarized microscopy system, on the one hand, the POM can be used to observe the microscopic morphology of a
218 specific position in the polymer material, and on the other hand, the microscopic morphology can be collected at the
219 same time. Scattering data of the location. The SAXS data and the POM image are mutually corroborated, which
220 enhances the persuasiveness of the characterization results.

221 **4 Conclusion**

222 In this paper, premised on the development trend of multi-scale structure characterization methods of polymer materials,
223 for the first time, a set of CRL-POM combined devices was built on a synchrotron radiation line station to realize the
224 scattering characterization based on optical micro-area resolution. The research methods and technical routes used
225 in this experiment have been tested many times. The feasibility of the experimental system has also been tested by
226 a variety of material research systems. The system can provide theoretical guidance for the molecular structure and
227 high-performance design of related materials in the industry. At the same time, it also provides a new characterization
228 platform for the SSRF small-angle X-ray scattering station, and a new combination structure characterization method
229 for internal and external teams conducting polymer crystal structural research.

230 **References**

- 231 [1] Buffet, A. *et al.* P03, the microfocus and nanofocus x-ray scattering (minaxs) beamline of the petra iii storage ring:
232 the microfocus endstation. *J Synchrotron Radiat* **19**, 647–53 (2012). URL <https://www.ncbi.nlm.nih.gov/pubmed/22713902>.
- 234 [2] Liu, W. J. *et al.* Short focal length kirkpatrick-baez mirrors for a hard x-ray nanoprobe. *Review of Scientific
235 Instruments* **76** (2005). URL <GotoISI>://WOS:000233569800024.

- 236 [3] Zeng, X. H. *et al.* Ellipsoidal and parabolic glass capillaries as condensers for x-ray microscopes. *Applied Optics*
237 **47**, 2376–2381 (2008). URL <Goto^{ISI}>://WOS:000256365000075.
- 238 [4] A. Snigirev*, I. S. . B. L., V. Kohnt. A compound refractive lens for focusing high-energy x-rays. *NATURE* (1996).
- 239 [5] Dudchik, Y. I. *et al.* Microspot x-ray focusing using a short focal-length compound refractive lenses. *Review of*
240 *Scientific Instruments* **75**, 4651–4655 (2004). URL <Goto^{ISI}>://WOS:000224962900046.
- 241 [6] Jun Xu, S. Z., Haimu Ye & Guo, B. Organization of twisting lamellar crystals in birefringent banded polymer
242 spherulites: A mini-review. *Crystals* **7** (2017).
- 243 [7] Lengeler, B. *et al.* Imaging by parabolic refractive lenses in the hard X-ray range. *Journal of Synchrotron Radiation*
244 **6**, 1153–1167 (1999). URL <https://doi.org/10.1107/S0909049599009747>.
- 245 [8] Als-Nielsen, J. & McMorrow, D. *Elements of Modern X-ray Physics* (Wiley, 2011). URL <https://books.google.co.jp/books?id=rlqlbowlTRMC>.
- 246 [9] Liu, J., Ye, H.-M., Xu, J. & Guo, B.-H. Formation of ring-banded spherulites of α and β modifications in
247 poly(butylene adipate). *Polymer* **52**, 4619–4630 (2011).